# Atomistic Sodiation Mechanism of a Phosphorene/Graphene Heterostructure for Sodium-Ion Batteries Determined by First-Principles Calculations

Hong Woo Lee, Hyun Jung, Byung Chul Yeo, Donghun Kim, and Sang Soo Han*

Computational Science Research Center, Korea Institute of Science and Technology (KIST), 5 Hwarangno 14-gil, Seongbuk-gu, Seoul 02792, Republic of Korea

Ⓢ *Supporting Information*

ABSTRACT: Black phosphorus has recently attracted significant attention as an anode material for sodium-ion batteries (SIBs); however, the material suffers from a severe volume change during charge/discharge processes, leading to poor cycle life. To overcome this drawback of black phosphorus, a phosphorene/graphene (P/G) heterostructure was recently proposed, but no atomistic understanding of the sodiation mechanism has yet been reported. In this work, we report an atomistic mechanism for the sodiation of the P/G hybrid material based on first-principles calculations. The layered structure of P/G is maintained up to the composition of $Na_{0.25}P/G$, which can be referred to as an intercalation process; however, above that composition, further sodiation

leads to the dissociation of P−P bonds and the formation of an amorphous Na_xP/G structure where the graphene layers are not broken and no Na atoms intercalate into the spaces between two graphene layers, which is referred to as an alloying process. According to our first-principles calculation, the graphene layers in the P/G material provide a buffer layer to accommodate the volume expansion of the material during sodiation (30% lower than that in the case of black phosphoros) without sacrificing the specific capacity. On the basis of calculations of carrier effective masses based on the band structures calculated by a hybrid density functional theory at the HSE06 level, the P/G material exhibits electrical conductivity superior to that of black phosphorus, in which graphene layers in the P/G can provide an electrical conducting channel even at a high sodiation level because the graphene layers are maintained up to full sodiation. Moreover, first-principles molecular dynamics simulations demonstrate that graphene layers in the P/G provide facile diffusion channels for Na atoms in highly sodiated Na_xP/G, although the effect is not significant during the intercalation process. On the basis of these results, we can expect that the P/G heterostructure has superior cycling properties and high rate capabilities and that the P/G hybrid material can indeed be a promising material for the anode of practical SIBs.
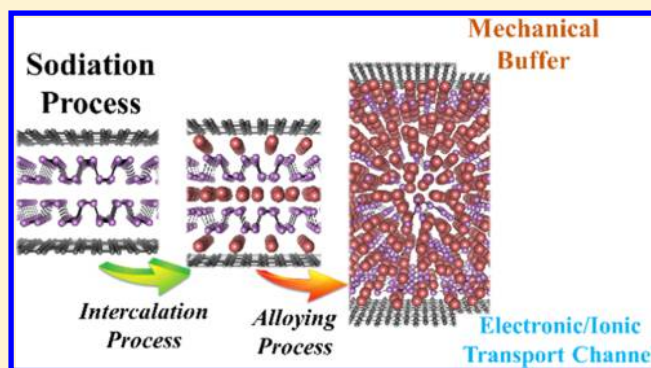
1. INTRODUCTION

Sodium-ion batteries (SIBs) have been regarded as a fascinating alternative to lithium-ion batteries (LIBs) because of the natural abundance of sodium and the similarity of the chemistries of sodium and lithium.[1−3] Additionally, it has been expected that the battery operating system of SIBs would be similar to that of LIBs. However, despite these advantages, several problems hinder the practical use of SIBs. In particular, the absence of an appropriate anode material is one of the most important problems.[4] Although graphite has been used as a representative anode material in LIBs, it is difficult for a sodium (Na) ion to intercalate into the interlayer spaces of graphite, which indicates that graphite is unsuitable as an anode material for SIBs.[5−7]

Recently, several studies have reported the potential of black phosphorus (BP) to serve an anode material for SIBs.[8] Among the three allotropes of phosphorus (red, white, and black), BP exhibits the highest chemical stability at the room temper-

ature.[9−11] Moreover, BP possesses a graphite-like layered structure consisting of phosphorene layers with an AB stacking pattern bound by van der Waals interactions. The interlayer distance of BP is greater than that of graphite (5.4 Å for BP vs 3.4 Å for graphite),[10−12] providing a channel through which Na ions can more easily intercalate into the layer spaces than in graphite. In addition, phosphorus has a remarkable theoretical specific capacity of 2596 mA h g^{-1} for Na_3P.[13−15] Indeed, BP shows a high experimental charge capacity (Na ion insertion) of 2035 mA h g^{-1}, although its reversible discharge capacity (Na ion removal) decreases to 637 mA h g^{-1}; nevertheless, both values are higher than those of amorphous red P (charge capacity: 897 mA h g^{-1} and discharge capacity: 15 mA h g^{-1}).[15] Despite these advantages, BP suffers from rapid
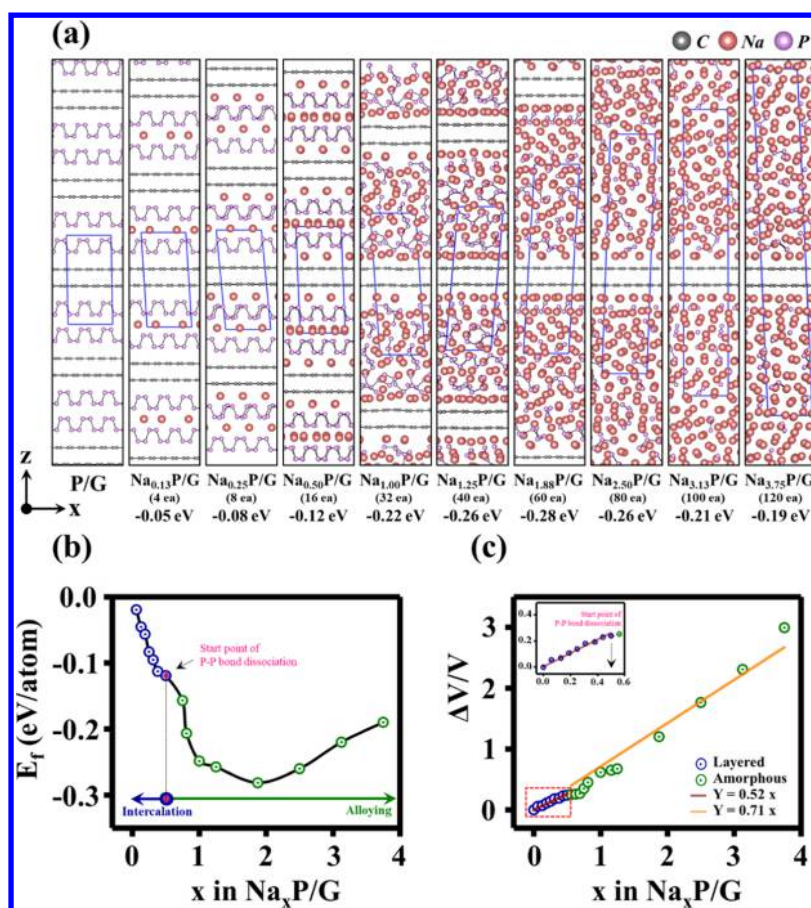
Figure 1. (a) Sodiation mechanism of the P/G heterostructure. Here, the numbers in parentheses indicate the numbers of Na atoms in the cell of the P/G, and the energies below each figure indicate the calculated formation energies of Na$_x$P/G structures. Color codes of atoms are gray = C, purple = P, and orange = Na. (b) Calculated formation energies and (c) volume expansion of Na$_x$P/G systems. The inset in (c) corresponds to data for the layered Na$_x$P/G region at low Na concentrations.

capacity fading, which is induced by a large volume change during charging/discharging processes.[16,17] To overcome this problem associated with BP, Sun et al.[16] proposed a phosphorene/graphene (P/G) heterostructured material. They experimentally synthesized a few phosphorene layers sandwiched between graphene layers and reported that the hybrid structure exhibited a specific capacity of 2440 mA h g^{-1} and an 83% capacity retention even after 100 cycles at the operating voltages of 0−1.5 V, which demonstrates that the P/G heterostructure has a great potential as an anode material for SIBs. Theoretically, using a first-principles calculation, Wang et al.[18] also reported on the potential of the P/G heterostructured material as an anode for SIBs. Additionally, for potential anode materials of LIBs, the P/G heterostructures were also theoretically proposed,[19] along with the pristine and defected phosphorene structures.[20,21]

Although the P/G material is promising for SIBs, there is a room for improvement regarding its practical use. In addition, to improve the battery performance of the P/G heterostructured material in SIBs, a thorough understanding of its sodiation mechanism at the atomic scale is critically important. In the present work, we report a comprehensive first-principles study on the sodiation mechanism of the P/G heterostructure up to a full sodium concentration at the atomic scale. In addition, we discuss the volume expansion behavior observed during sodiation and the electrical conductivity and diffusivity

of the P/G heterostructure, which must be considered for anode applications.

2. COMPUTATIONAL DETAILS

First-principles calculations were carried out using a periodic density functional theory (DFT) framework in the Vienna Ab initio Simulation Package software.[22,23] To describe the exchange-correlation energy, we employed the generalized gradient approximation proposed by Perdew−Burke−Ernzer-hof.[24] The effects of core electrons were replaced with projector augmented wave potentials.[25] The electronic wave functions were expanded on a plane-wave basis set with a kinetic energy cutoff of 400 eV. To consider the van der Waals interactions between layers in the P/G heterostructure, we additionally adopted Grimme's DFT-D2 method.[26]

To explore Na incorporation and diffusion, we modeled a P/G heterostructure containing 32 phosphorus atoms and 48 carbon atoms, whose structure consisted of two phosphorene and two graphene layers (four layers in total). We also investigated the stacking effect of phosphorene (P) and graphene (G) layers in the P/G heterostructure, determining that the P/P/G/G stacking order is thermodynamically more favorable than the P/G/P/G stacking order, as shown in Figure S1 of the Supporting Information. Thus, in this work, the P/G heterostructure with P/P/G/G stacking was considered for Na incorporation and diffusion. The optimized cell parameters of the heterostructure were a = 7.26 Å, b = 8.53
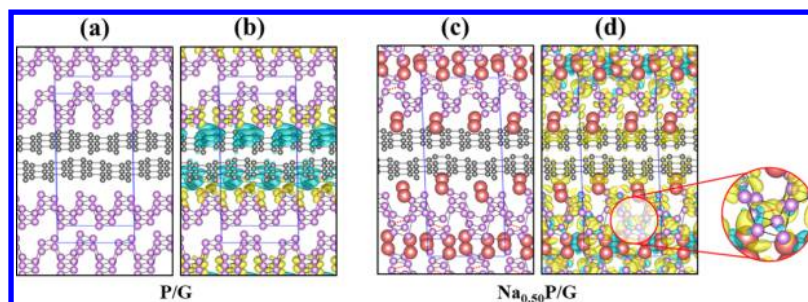
Figure 2. Side views (a,c) and charge density difference plots (b,d) of optimized P/G (a,b) and $Na_{0.50}P/G$ (c,d) structures. The red circle in (d) highlights the region in which the P—P bond dissociation (red line) occurs. The yellow and cyan colors in (b,d) indicate charge accumulation and depletion, respectively.

Å, and c = 16.97 Å. The Brillouin zone was sampled using a 6 × 4 × 2 Monkhorst–Pack mesh.[27] The atomic structures of Na_xP/G ($0 \leq x \leq 3.75$) were fully optimized with no symmetry constraint. For structural optimization, atomic positions and cell sizes were optimized until the energy change was less than 10^{-6} eV between two consecutive self-consistent steps, and the forces on the atoms were less than 0.02 eV Å^{-1}. Detailed information on the optimized Na_xP/G structures is summarized in Table S1.

To examine the Na diffusion properties in the P/G heterostructure during the early stages of sodiation, we performed a climbing image nudged elastic band (CI-NEB) calculation.[28] The initial reaction path was constructed by a linear interpolation between the atomic coordinates based on six images, and the structures were then relaxed until the force on each atom was smaller in magnitude than 0.02 eV/Å. To further investigate the diffusivity of Na in the heterostructure at high sodium concentrations, an ab initio molecular dynamics (AIMD) simulation was additionally performed under the control of a Nosé–Hoover thermostat with a molecular dynamics (MD) time step of 1 fs, where the MD temperature was assumed to be 800 K to accelerate the movements of atoms.

Moreover, we investigated the electrical conductivity of the P/G heterostructure through calculations of effective carrier masses based on the electronic band structure of the heterostructure, in which the Heyd–Scuseria–Ernzerhof (HSE06)[29] hybrid functional method was considered. Then, we compared the effective carrier masses of the P/G heterostructure with those of BP.

3. RESULTS AND DISCUSSION

3.1. Sodiation Mechanism in the P/G Heterostructure. To determine the sodiation mechanism of the P/G heterostructure at the atomic scale, we calculated the formation energies of sodiated P/G (Na_xP/G) structures as a function of the sodiation concentration (x) using the following equation

$$E_f(x) = [E_{tot}(Na_xP/G) - E_{tot}(P/G) - xE_{tot}(Na)]/x \tag{1}$$

where $E_{tot}(Na_xP/G)$ is the total energy of the sodiated P/G heterostructure, $E_{tot}(P/G)$ is the total energy of the P/G heterostructure, and $E_{tot}(Na)$ is the total energy per atom in the body-centered cubic Na crystal. The P/G heterostructure contains 32 phosphorus atoms and 48 carbon atoms, leading to the composition of $P_{32}C_{48}$ ($PC_{1.5}$). According to eq 1, a negative formation energy implies a thermodynamically

favorable process for sodiation. For a given x of Na_xP/G, we considered various atomic configurations, optimized the systems with full structural relaxation, and selected the optimized structures to clarify the sodiation mechanism. In addition, we considered sodiation concentrations (x) up to $Na_{3.75}P/G$, whose atomic structure included 120 Na atoms.

Figure 1a shows an atomistic mechanism of the P/G heterostructure based on the calculated formation energies (Figure 1b). During the early stages of sodiation (e.g., $Na_{0.13}P/G$), Na atoms energetically prefer to locate between the P/P interlayers rather than between the P/G or G/G interlayers (Figure S2), where they occupy the same P/P interlayer space up to θ = 25% coverage per phosphorene layer. Beyond this coverage, additional Na atoms are located between the P/G interlayers. However, although sodiation continues to proceed, no Na atom is intercalated in the G/G interlayer space. We also found that there is no P—P bond dissociation in the P/G heterostructure at Na concentrations below $Na_{0.25}P/G$, which indicates that sodiation can be considered as an intercalation process. At the Na concentration of $Na_{0.50}P/G$, P—P bond dissociation occurs, and the dissociated P atoms are alloyed with Na atoms. Under these conditions, such a change in the sodiation mechanism is also observed in BP.[30] Moreover, even during the alloying process, it is also observed that no Na atom intercalates into the two graphene layer spaces and that no C—C bond dissociation occurs in the graphene layers.

According to Figure 1b, the maximum Na storage content in the P/G heterostructure is approximately $Na_{1.88}P/G$, corresponding to a specific capacity of 2565 mA h g^{-1}, which is similar to the theoretical specific capacity of phosphorus (Na_3P: 2596 mA h g^{-1}).[16] Indeed, Sun et al.[16] experimentally reported that P/G hybrid structures show an initial capacity of ~2050 mA h g^{-1} at a carbon/phosphorus C/P mole ratio = 1.39 and an initial capacity of ~2300 mA h g^{-1} at C/P = 2.07, which are similar to our DFT prediction (2565 mA h g^{-1} for $Na_{1.88}P/G$, where the P/G has a C/P ratio of 1.5). In addition, we investigated the volume expansion behaviors of the P/G heterostructure during sodiation (Figure 1c). According to our previous DFT calculation regarding the sodiation of BP,[30] the volume expansion ($\Delta V/V_o$) of BP increases linearly with Na concentration, although the sodiation mechanism changes from an intercalation process to an alloying process, that is, the slope of $\Delta V/V_o$ versus x in Na_xP is 1.06 for the intercalation process and 1.05 for the alloying process. In contrast, in the P/G heterostructure, the volume expansion (slope: 0.52) during the intercalation process is smaller than that (slope: 0.71) in the alloying process. In addition, it is observed that the slopes are 30–50% smaller than those[30] observed for BP, which
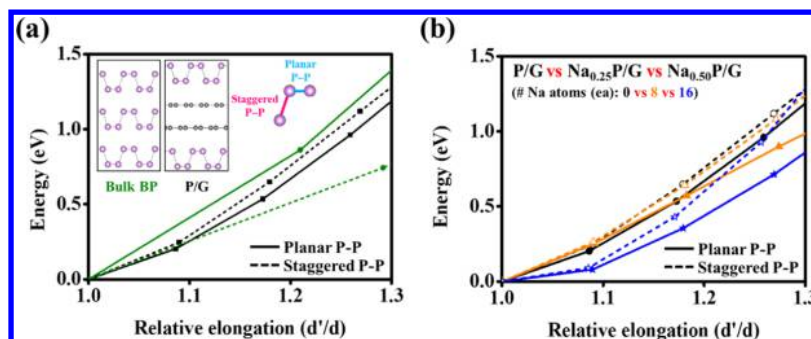
Figure 3. (a) Comparison of energy profiles with elongation (d'/d) of planar (solid line) and staggered (dotted line) P−P bonds in BP (green) and the P/G (black), where d is an optimized P−P bond distance and d' is an elongated bond distance. The results for BP are from ref 30. Here, the inset corresponds to atomistic structures of BP and the P/G heterostructures. Planar and staggered P−/P bonds in a phosphorene layer are also represented. (b) Energy profiles with elongation of planar (solid line) and staggered (dotted line) P−P bonds of Na_xP/G systems (x = 0.00, 0.25, and 0.50).

clearly indicates that graphene layers in the P/G heterostructure provide a buffer effect to accommodate the volume expansion of BP during a sodiation reaction. This effect results from the superior elastic properties of graphene layers, as no C−C bond in the graphene layers is broken during sodiation.

3.2. Investigating P−P Bond Breaking Mechanism in the Heterostructures. As indicated in Figure 1a, during the early stages of sodiation (e.g., $Na_{0.13}P/G$), Na atoms energetically prefer to locate between the P/P interlayers rather than between the P/G or G/G interlayers. To clarify the reason, we calculated the charge density difference ($\Delta\rho$) of the P/G heterostructure (Figure 2a) as follows

$$\Delta\rho = \rho_{P/G} - \rho_P - \rho_G \tag{2}$$

where $\rho_{P/G}$ is the electron density of the phosphorous/graphite heterostructure and ρ_P and ρ_G are the electron densities of pristine phosphorus and pristine graphite with the same atomic positions as the heterostructure, respectively.

In Figure 2b, a net gain of electronic charge is observed around the P atoms adjacent to the graphene layers, and a net loss is observed around the C atoms. This behavior implies that charge transfer occurs from the graphene layers to the adjacent phosphorene layers, generating a strong electrostatic interaction between the graphene and phosphorene layers. Intercalation of Na atoms into layered structures involves an increase in the interlayer spaces. Thus, the strong interaction between the phosphorene and graphene layers in the P/G heterostructure makes the intercalation of Na atoms into the P/G interlayer space more difficult than that into the P/P interlayer space, which clearly supports the preferential intercalation of Na atoms into the P/P interlayer spaces rather than the P/G interlayer spaces (Figures 1a and S2).

In Figure 1a, the intercalation process associated with sodiation with no P−P bond breaking occurs up to the composition of $Na_{0.25}P/G$; however, at $Na_{0.50}P/G$, P−P bond dissociation begins to occur. Thus, we also examined the P−P bond dissociation mode in the P/G heterostructure during sodiation. Phosphorene has a corrugated structure with two different types of P−P bonds: planar P−P (bond distance: 2.22 Å) and staggered P/− (bond distance: 2.26 Å).[30] In the case of BP, sodiation leads to the preferential breaking of staggered P−P bonds rather than that of planar P−P bonds.[30] However, in the P/G heterostructure, the dissociation of planar P−P bonds is preferred (Figure S3). Further sodiation of four Na atoms into $Na_{0.25}P/G$, corresponding to $Na_{0.50}P/G$, occurs in

the P/P interlayer space rather than in the P/G or G/G interlayer spaces, in which several planar P−P bonds in the P−P layer space are dissociated. To clarify the dissociation mode, we additionally calculated the charge density difference ($\Delta\rho$) for $Na_{0.50}P/G$ (Figure 2d) using the following equation

$$\Delta\rho = \rho_{Na_{0.50}P/G} - \rho_{P/G} - \rho_{Na} \tag{3}$$

where $\rho_{Na_{0.50}P/G}$, $\rho_{P/G}$, and ρ_{Na} are the electron densities of $Na_{0.50}P/G$ and the P/G heterostructure consisting of P and C atoms in the same positions observed in the $Na_{0.50}P/G$ system and the contribution from individual Na atoms in the positions they occupy in each $Na_{0.50}P/G$ system, respectively. A careful examination of a position close to where P−P bond dissociation occurs revealed significant charge transfer from Na atoms to the dissociated planar P−P bonds. The charge transfer generates a repulsion between the planar P−P bonds; ultimately, the bonds are dissociated.

To further confirm the dissociation mode of P−P bonds from a mechanical viewpoint, we calculated the energy changes of the Na_xP/G structures as a function of the change in the bond distance for the staggered and planar P−P bonds in Figure 3. In calculating the energy change, we optimized the Na_xP/G structures in conjunction with cell optimization, in which the positions of two P−P bond atoms were fixed at a given bond distance, whereas the other P, C, and Na atoms were allowed to relax. Figure 3a shows the energy profiles as a function of P−P bond elongation in bulk BP and the P/G heterostructure. For P/G, the slope of a staggered P−P bond is steeper than that of a planar one, which means that more energy is required to break staggered P−P bonds than planar P−P bonds. Figure 3b shows the energy profiles as a function of P−P bond elongation for the P/G, $Na_{0.25}P/G$, and $Na_{0.50}P/G$ systems. As sodiation proceeds, the slopes of the planar and staggered bonds decrease, indicating that it is easier to break P−P bonds in sodiated Na_xP/G structures than it is to break those in P/G. In addition, irrespective of the degree of sodiation in the P/G heterostructure, dissociation of planar P−P bonds is easier than that of staggered P−P bonds. Dissociation of the staggered P−P bonds leads to volume expansion geometrically along the z-axis rather than along the x- or y-axis, whereas for the dissociation of planar P−P bonds, the opposite is true. Graphene layers in the P/G heterostructure can help suppress volume expansion of the hybrid material during sodiation, as indicated in Figure 1c, in particular, volume expansion along the z-direction relative to
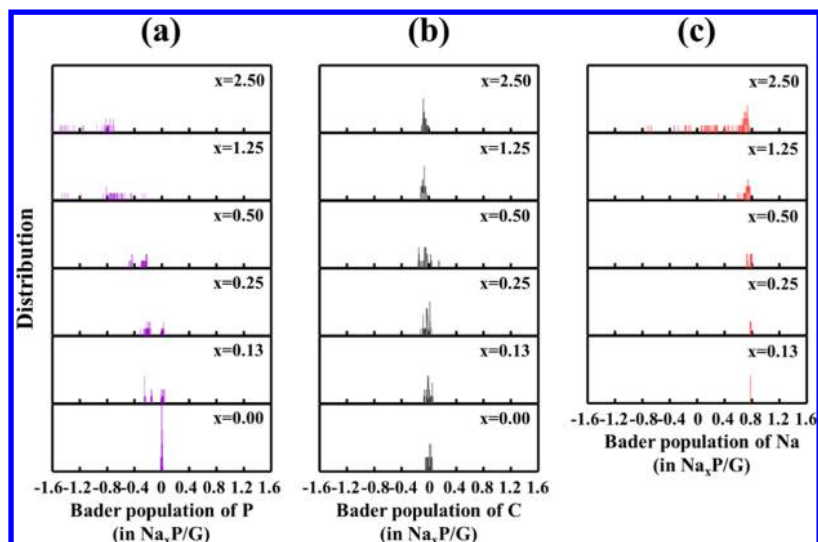
Figure 4. Distribution histograms of the Bader populations of (a) phosphorus, (b) carbon, and (c) sodium elements in Na_xP/G (x = 0.00, 0.13, 0.25, 0.50, 1.25, and 2.50).

the case of BP. Accordingly, the introduction of graphene layers can mechanically help preferentially dissociate the planar P−P bonds rather than the staggered ones.

To clarify the sodiation mechanism of the P/G heterostructure, we additionally performed a Bader charge analysis[31] of Na_xP/G as a function of Na content. Figure 4 shows the distribution histograms for the Bader atomic charge population of phosphorus, carbon, and sodium in Na_xP/G. The atomic charges of carbon atoms in Na_xP/G do not change significantly during sodiation, whereas those of phosphorus atoms do. This discrepancy indicates that Na atoms interact with P atoms more strongly than C atoms do. In contrast, the atomic charges of Na maintain a constant value of +0.78e up to $Na_{0.25}P/G$, supporting the intercalation mechanism. However, above the composition of $Na_{0.50}P/G$, the charge states of Na decrease rapidly, and atomic charge values vary widely because of the formation of amorphous Na_xP/G structures from the P−P bond dissociation induced by sodiation, which is also observed in the case of BP.[17] Interestingly, in highly sodiated structures (e.g., $Na_{1.25}P/G$ or $Na_{2.50}P/G$), several Na atoms have negative atomic charge states, which results from local clustering of the Na atoms.

3.3. Electrical Conductivities of the P/G Heterostructures. The electrical conductivity of the electrode materials in rechargeable batteries also determines the cycling properties of the batteries. In this regard, we also investigated the electrical conductivity of the P/G heterostructure and then compared it with that of BP by calculating effective masses of carriers based on the respective band structures of the materials.

Figure 5 shows the band structures of BP and P/G calculated by a hybrid DFT method at the level of the HSE06 functional. According to a previous study,[32] the HSE06 functional provides a more accurate band gap for BP than other DFT methods do. In addition, our HSE06 calculation yields a band gap of 0.25 eV at the Γ point, which is similar to the previously reported HSE06 result (0.27 eV).[32] For the P/G heterostructure, our HSE06 calculation reveals a nearly direct band gap of 0.10 eV near the Γ point; the band gap is narrower than that of bulk BP because of the introduction of graphite layers.
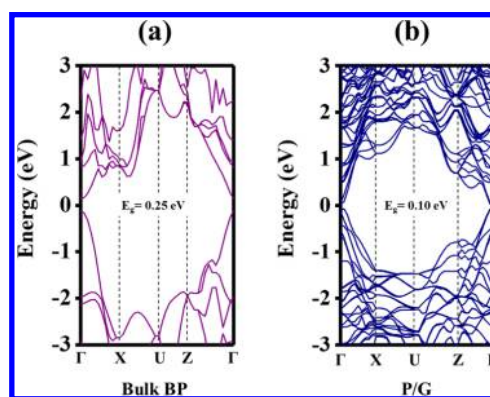

Figure 5. Electronic band structures of (a) pristine BP and (b) the P/G heterostructure using the HSE06 functional. The band structures are plotted along Γ (0, 0, 0) → X (0.5, 0, 0) → U (0.5, 0, 0.5) → Z (0, 0, 0.5) → Γ (0, 0, 0). In addition, the corresponding band gap values are also represented in each figure.

To compare the transport properties of carriers in the BP and the P/G heterostructure, based on the HSE06 band structures shown in Figure 5, we calculated the effective masses (m^*) of electrons and holes in the two materials by using the following equation[33]

$$(m^*)^{-1} = \frac{1}{\hbar^2} \frac{\partial^2 E}{\partial k^2} \tag{4}$$

where E is the energy of a band as a function of the wave vector k and $\hbar$ is the reduced Planck constant. According to eq 4, the effective mass is inversely proportional to the curvature of the $E-k$ dispersion: high curvature leads to a small mass and thus fast carrier transport.

Table 1 presents the effective masses of carriers obtained from the band structures for BP and P/G. In BP, the effective masses of both electrons and holes along Γ−X are substantially greater than those along the Γ−Y direction: $0.64m_0(\Gamma-X) \gg 0.16m_0(\Gamma-Y)$ for holes and $1.15m_0(\Gamma-X) \gg 0.12m_0(\Gamma-Y)$ for electrons. Such an anisotropic feature is consistent with the results reported in a previous study.[34] However, the effective masses in the P/G hybrid material are isotropic and extremely small along arbitrary directions in the xy-plane. For example,

Table 1. Effective Masses of Holes (m_h^*) and Electrons (m_e^*) in Pristine BP and the P/G Heterostructure, Obtained Based on the Band Structures Shown in Figure 5

	direction	bulk BP	P/G
m_h^*	$\Gamma - X$	$0.64m_0$	$0.07m_0$
	$\Gamma - Y$	$0.16m_0$	$0.07m_0$
m_e^*	$\Gamma - X$	$1.15m_0$	$0.06m_0$
	$\Gamma - Y$	$0.12m_0$	$0.08m_0$

the effective masses of holes are $0.07m_0$ along both the $\Gamma - X$ and $\Gamma - Y$ directions; similarly, the masses of electrons range from 0.06 to $0.08m_0$. This isotropic behavior is attributed to the fact that band edge states of the P/G material are predominantly determined by C $2p_z$ orbitals. In addition, the introduction of graphene layers into BP significantly reduces the effective masses of both electrons and holes by approximately 16-fold, providing significantly enhanced electrical conductivity, as observed in a previous experiment.[16] As previously explained with respect to Figure 1, the graphene layers are never been broken during sodiation, although high sodiation leads to the dissociation of P−P bonds in phosphorene layers. This finding reveals that electrical conducting channels in the P/G heterostructure are maintained even at the full sodiation level, which can allow for superior cycling performance of the P/G material.

3.4. Diffusion of Na Atoms in P/G Heterostructures.
The diffusion properties of Na atoms also represent a key factor in determining the anode properties of SIBs, in particular, charge/discharge rates and power densities. Thus, we also investigated the diffusion behaviors of the two test materials during intercalation and alloying. For the intercalation process, we calculated the diffusion energy barriers of Na by the CI-NEB method, in which we considered diffusion pathways of a single Na atom in the P/P interlayer space and the P/G space, as shown in Figure 6a.

According to our previous DFT studies,[17,30] a Na atom in BP shows one-dimensional diffusion behavior along the same pore channel direction; thus, we focused on the diffusion path in this work (Figure 6a). The results of our CI-NEB calculations presented in Figure 6b reveal that the Na diffusion barriers in the P/P and P/G interlayer spaces are similar: 0.22 eV for the P/P space and 0.25 eV for the P/G space. This result indicates that as the interlayer mechanism proceeds (Na concentration is low), Na diffusion in the P/G heterostructure is facile; however, during that process, the introduction of graphene layers does not provide a significant enhancement in Na diffusion.

To examine the effect of the graphene layer on Na diffusivities during the alloying process, we additionally performed AIMD simulations of the $Na_{1.00}P/G$ system (Figure 6c). From the AIMD trajectories of Na atoms, we calculated their mean square displacements (MSDs) with the following equation, $MSD = |R_i(t) - R_i(0)|^2$, where $R_i(t)$ is the position of the Na atom i at time t. The MSD results are shown in Figure 6d. The Na diffusivity (D_{Na}) was then obtained by using the Einstein relation, $D = MSD/nt$, where $n = 6$ for three-dimensional diffusion at time t. We calculated the diffusivity of Na near graphene relative to the corresponding diffusivity in the $Na_{1.00}P/G$ bulk system. Figure 6d clearly shows that the diffusion of Na atoms near graphene is faster than that in the alloy bulk. At 800 K, the Na diffusivity (D_{Na}) near the graphene layer is 2.6×10^{-6} cm^2/s, which is 2.6 times greater
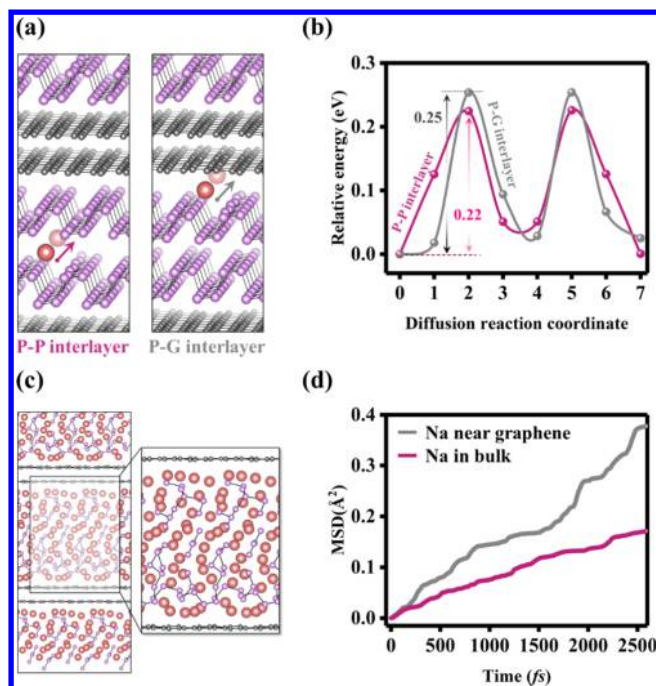

Figure 6. (a) Diffusion behavior of a Na atom in the P/P or P/G interlayer space in the P/G heterostructure and (b) NEB diffusion paths of each Na atom. (c) Atomistic structure of the $Na_{1.00}P/G$ system and (d) MSDs for Na atoms in the $Na_{1.00}P$ system determined from AIMD simulations, where a gray line corresponds to Na atoms near interfaces between $Na_{1.00}P$ and graphene and a red line corresponds to Na atoms in the bulk.

than $D_{Na} = 1.0 \times 10^{-6}$ cm^2/s in the bulk. During the alloying process of sodiation, Na atoms in the Na_xP/G bulk strongly interact with P atoms or P−P dumbbells, and Na clusters are formed, which leads to low diffusivities.[35] According to these results, the introduction of graphene layers into the phosphorene layers can not only enhance electrical conductivity but can also improve the diffusivity of Na atoms (ionic conductivity), particularly at the high sodiation level that occurs during the alloying sodiation mechanism.

4. CONCLUSIONS
In conclusion, the present DFT work provides a systematic description of sodiation of the P/G heterostructure at the atomic scale. According to our DFT calculations, the P/G hybrid material overall shows a sodiation mechanism similar to that of BP, in which sodiation proceeds via an intercalation mechanism first up to $Na_{0.25}P/G$ with no P−P bond dissociation; then, at higher Na concentrations, the alloying process proceeds with rigorous P−P bond dissociation but with no C−C bond breaking in graphene layers. However, in comparison with BP, the P/G heterostructure offers several beneficial effects as an anode material. In particular, the introduction of graphene layers into BP can suppress the volume expansion of the P/G material during sodiation without sacrificing specific capacity. In addition, the graphene layers in the P/G hybrid material enhance the electrical conductivity of the material beyond that of BP during full sodiation. Moreover, the graphene layer provides a facile diffusion channel for Na atoms in highly sodiated Na_xP/G structures. On the basis of these results, it is expected that the P/G heterostructure possesses superior cycling properties and high rate capabilities, as observed in a previous experiment.[16]

Our DFT calculations clearly reveal that the P/G hybrid material can indeed be a promising anode material for practical SIBs.

ASSOCIATED CONTENT

S Supporting Information

The Supporting Information is available free of charge on the ACS Publications website at DOI: 10.1021/acs.jpcc.8b06742.

Additional DFT results on the sodiation mechanism (PDF)

AUTHOR INFORMATION

Corresponding Author
*E-mail: sangsoo@kist.re.kr. Phone.: +82 2 958 5441. Fax: +82 2 958 5451.

ORCID
Donghun Kim: 0000-0003-0326-5381
Sang Soo Han: 0000-0002-7925-8105

Notes
The authors declare no competing financial interest.

ACKNOWLEDGMENTS

REFERENCES

(1) Kim, S.-W.; Seo, D.-H.; Ma, X.; Ceder, G.; Kang, K. Electrode Materials for Rechargeable Sodium-Ion Batteries: Potential Alternatives to Current Lithium-Ion Batteries. *Adv. Energy Mater.* **2012**, 2, 710−721.

(2) Liang, Y.; Lai, W.-H.; Miao, Z.; Chou, S.-L. Nanocomposite Materials for the Sodium-Ion Battery: A Review. *Small* **2018**, 14, 1702514.

(3) Slater, M. D.; Kim, D.; Lee, E.; Johnson, C. S. Sodium-Ion Batteries. *Adv. Funct. Mater.* **2013**, 23, 947−958.

(4) Cui, J.; Yao, S.; Kim, J.-K. Recent Progress in Rational Design of Anode Materials for High-Performance Na-Ion Batteries. *Energy Storage Mater.* **2017**, 7, 64−114.

(5) Ellis, B. L.; Nazar, L. F. Sodium and Sodium-Ion Energy Storage Batteries. *Curr. Opin. Solid State Mater. Sci.* **2012**, 16, 168−177.

(6) Wen, Y.; He, K.; Zhu, Y.; Han, F.; Xu, Y.; Matsuda, I.; Ishii, Y.; Cumings, J.; Wang, C. Expanded Graphite as Superior Anode for Sodium-Ion Batteries. *Nat. Commun.* **2014**, 5, 4033.

(7) Lee, H. W.; Moon, H. S.; Hur, J.; Kim, I. T.; Park, M. S.; Yun, J. M.; Kim, K. H.; Lee, S. G. Mechanism of sodium adsorption on N-doped graphene nanoribbons for sodium ion battery applications: A density functional theory approach. *Carbon* **2017**, 119, 492−501.

(8) Sun, L.-Q.; Li, M.-J.; Sun, K.; Yu, S.-H.; Wang, R.-S.; Xie, H.-M. Electrochemical Activity of Black Phosphorus as an Anode Material for Lithium-Ion Batteries. *J. Phys. Chem. C* **2012**, 116, 14772−14779.

(9) Wang, L.; He, X.; Li, J.; Sun, W.; Gao, J.; Guo, J.; Jiang, C. Nano-Structured Phosphorus Composite as High-Capacity Anode Materials for Lithium Batteries. *Angew. Chem., Int. Ed.* **2012**, 51, 9034−9037.

(10) Hultgren, R.; Gingrich, N. S.; Warren, B. E. The Atomic Distribution in Red and Black Phosphorus and the Crystal Structure of Black Phosphorus. *J. Chem. Phys.* **1935**, 3, 351−355.

(11) Morita, A. Semiconducting Black Phosphorus. *Appl. Phys. A* **1986**, 39, 227−242.

(12) Bacon, G. E. The Interlayer Spacing of Graphite. *Acta Crystallogr.* **1951**, 4, 558−561.

(13) Stan, M. C.; von Zamory, J.; Passerini, S.; Nilges, T.; Winter, M. Puzzling Out the Origin of the Electrochemical Activity of Black P as a Negative Electrode Material for Lithium-Ion Batteries. *J. Mater. Chem. A* **2013**, 1, 5293−5300.

(14) Li, W.-J.; Chou, S.-L.; Wang, J.-Z.; Liu, H.-K.; Dou, S.-X. Simply Mixed Commercial Red Phosphorus and Carbon Nanotube Composite with Exceptionally Reversible Sodium-Ion Storage. *Nano Lett.* **2013**, 13, 5480−5484.

(15) Qian, J.; Wu, X.; Cao, Y.; Ai, X.; Yang, H. High Capacity and Rate Capability of Amorphous Phosphorus for Sodium Ion Batteries. *Angew. Chem., Int. Ed.* **2013**, 52, 4633−4636.

(16) Sun, J.; Lee, H.-W.; Pasta, M.; Yuan, H.; Zheng, G.; Sun, Y.; Li, Y.; Cui, Y. A Phosphorene-Graphene Hybrid Material as a High-Capacity Anode for Sodium-Ion Batteries. *Nat. Nanotechnol.* **2015**, 10, 980−985.

(17) Hembram, K. P. S. S.; Jung, H.; Yeo, B. C.; Pai, S. J.; Lee, H. J.; Lee, K.-R.; Han, S. S. A Comparative First-Principles Study of the Lithiation, Sodiation, and Magnesiation of Black Phosphorus for Li-, Na-, and Mg-Ion Batteries. *Phys. Chem. Chem. Phys.* **2016**, 18, 21391−21397.

(18) Wang, L.; Jiang, Z.; Li, W.; Gu, X.; Huang, L. Hybrid Phosphorene/Graphene Nanocomposite as an Anode Material for Na-Ion Batteries: A First-Principles Study. *J. Phys. D: Appl. Phys.* **2017**, 50, 165501.

(19) Guo, G.-C.; Wang, D.; Wei, X.-L.; Zhang, Q.; Liu, H.; Lau, W.-M.; Liu, L.-M. First-Principles Study of Phosphorene and Graphene Heterostructure as Anode Materials for Rechargeable Li Batteries. *J. Phys. Chem. Lett.* **2015**, 6, 5002−5008.

(20) Guo, G.-C.; Wei, X.-L.; Wang, D.; Luo, Y.; Liu, L.-M. Pristine and Defect-Containing Phosphorene as Promising Anode Materials for Rechargeable Li Batteries. *J. Mater. Chem. A* **2015**, 3, 11246−11252.

(21) Wang, D.; Guo, G.-C.; Wei, X.-L.; Liu, L.-M.; Zhao, S.-J. Phosphorene Ribbons as Anode Materials with Superhigh Rate and Large Capacity for Li-Ion Batteries. *J. Power Sources* **2016**, 302, 215−222.

(22) Kresse, G.; Furthmüller, J. Efficient Iterative Schemes for Ab Initio Total-Energy Calculations Using a Plane Wave Basis Set. *Phys. Rev. B: Condens. Matter Mater. Phys.* **1996**, 54, 11169−11186.

(23) Kresse, G.; Furthmüller, J. Efficiency of Ab-Initio Total Energy Calculations for Metals and Semiconductors Using a Plane-Wave Basis Set. *Comput. Mater. Sci.* **1996**, 6, 15−50.

(24) Perdew, J. P.; Burke, K.; Ernzerhof, M. Generalized Gradient Approximation Made Simple. *Phys. Rev. Lett.* **1996**, 77, 3865−3868.

(25) Blöchl, P. E. Projector Augmented-Wave Method. *Phys. Rev. B: Condens. Matter Mater. Phys.* **1994**, 50, 17953−17979.

(26) Grimme, S. Semiempirical GGA-Type Density Functional Constructed with a Long-Range Dispersion Correction. *J. Comput. Chem.* **2006**, 27, 1787−1799.

(27) Monkhorst, H. J.; Pack, J. D. Special Points for Brillouin-Zone Integrations. *Phys. Rev. B: Condens. Matter Mater. Phys.* **1976**, 13, 5188−5192.

(28) Henkelman, G.; Uberuaga, B. P.; Jónsson, H. A Climbing Image Nudged Elastic Band Method for Finding Saddle Points and Minimum Energy Paths. *J. Chem. Phys.* **2000**, 113, 9901−9904.

(29) Krukau, A. V.; Vydrov, O. A.; Izmaylov, A. F.; Scuseria, G. E. Influence of the Exchange Screening Parameter on the Performance of Screened Hybrid Functionals. *J. Chem. Phys.* **2006**, 125, 224106.

(30) Hembram, K. P. S. S.; Jung, H.; Yeo, B. C.; Pai, S. J.; Kim, S.; Lee, K.-R.; Han, S. S. Unraveling the Atomistic Sodiation Mechanism of Black Phosphorus for Sodium Ion Batteries by First-Principles Calculations. *J. Phys. Chem. C* **2015**, 119, 15041−15046.

(31) Sanville, E.; Kenny, S. D.; Smith, R.; Henkelman, G. Improved Grid-Based Algorithm for Bader Charge Allocation. *J. Comput. Chem.* **2007**, 28, 899−908.

(32) Qiao, J.; Kong, X.; Hu, Z.-X.; Yang, F.; Ji, W. High-Mobility Transport Anisotropy and Linear Dichroism in Few-Layer Black Phosphorus. *Nat. Commun.* **2014**, 5, 4475.

(33) Kim, D.; Yeo, B. C.; Shin, D.; Choi, H.; Kim, S.; Park, N.; Han, S. S. Dissimilar Anisotropy of Electron Versus Hole Bulk Transport in

Anatase TiO$_2$: Implications for Photocatalysis. *Phys. Rev. B* **2017**, *95*, 045209.

(34) Li, Y.; Yang, S.; Li, J. Modulation of the Electronic Properties of Ultrathin Black Phosphorus by Strain and Electrical Field. *J. Phys. Chem. C* **2014**, *118*, 23970−23976.

(35) Yeo, B. C.; Jung, H.; Lee, H. W.; Yun, K.-S.; Kim, H.; Lee, K.-R.; Han, S. S. Atomistic Simulation Protocol for Improved Design of Si-O-C Hybrid Nanostructures as Li-Ion Battery Anodes: ReaxFF Reactive Force Field. *J. Phys. Chem. C* **2017**, *121*, 23268−23275.